Indian Journal of Pure & Applied Physics
Vol. 62, November 2024, pp. 984-995
DOI: 10.56042/ijpap.v62i11.10341

Compact Dual Band Substrate Integrated Waveguide MIMO Antenna for X-Band Application

Inderpreet Kaur[a], Banani Basu[b] & Anil Kumar Singh[c]

[a]Department of Electronics and Communication Engineering, Mahatma Jyotiba Phule Rohilkhand University, Bareilly 243 006, India
[b]Department of Electronics and Communication Engineering, NIT Silchar, Assam, 788 010, India
[c]Department of Electronics and Instrumentation Engineering, Mahatma Jyotiba Phule Rohilkhand University, Bareilly 243 006, India

Received 20 April 2024; accepted 10 October 2024

This article introduces a compact, dual-band, eight-port Multiple Input Multiple Output (MIMO) stacking antenna integrated with Substrate Integrated Waveguide (SIW) and a common ground. The antenna operates in the 9.2-9.5 GHz and 11.5-12.25 GHz frequency bands. Its configuration consists of four identical, coaxial fed annular ring radiators mounted on an FR4 substrate (40x40x4 mm^3). To enhance the performance of the eight-port MIMO antenna, a feed structure is positioned above the radiator structure. The SIW-integrated MIMO antenna demonstrates excellent isolation (>15 dB), high gain (8 dB and 6.6 dB), and favourable diversity parameters. The design demonstrates a minimal Envelope Correlation Coefficient (ECC) of 0.10 and a substantial diversity gain (DG) of 9.96 dB, demonstrating its potential to guarantee strong diversity reception and improve communication dependability, especially in challenging situations.

Keywords: Substrate integrated waveguide (SIW); Multiple Input Multiple Output (MIMO); Envelope correlation Coefficient (ECC)

1 Introduction

In recent years, multiple-input multiple-output (MIMO) technology has garnered considerable attention for its capability to boost data throughput and extend transmission range without requiring additional bandwidth or increased transmit power[1]. Various decoupling methods for MIMO arrays have been explored, including placement of feed lines i.e. orthogonally and integration of metallic strip between the elements[2] defected ground structure[3], parasitic decoupling[4], and energy cancellation[5]. Moreover, the use of metasurfaces (MS) as an efficient decoupling technology has been investigated[6]. Another effective decoupling approach is presented in[7], involving a simple yet efficient feeding network for suppressing mutual coupling between two substrate-integrated waveguides (SIW) slot antenna arrays. This method employs a two-layer directional coupler connected directly to the SIW-slot antenna arrays, establishing controlled magnitude and phase indirect coupling. Importantly, this proposed feeding network occupies minimal space and has negligible impact on return loss and radiation patterns. In[8] A novel method for achieving broadband operating bandwidth and minimizing cross-polarization radiation in a stacked SIW microstrip patch antenna is introduced. It uses three stacked PCB layers: one for radiating patch elements and two for the SIW PCB layers housing the feeding network. A study evaluates a parasitic structure's impact on a four-element MIMO antenna's performance. Another technique employs eight layers having feeding structure and radiating structure on different layers[9].

Initially designed as a square-shaped patch antenna operating from 4.5 to 5.8 GHz, it's duplicated orthogonally for a broader bandwidth. A parasitic structure enhances isolation, with improved minimum as well as maximum isolation of 20 dB and 45 dB[10]. Four-element CPWG fed MIMO antenna for WiFi. With an inverted-C structure atop Y-shaped monopoles, it creates a 4-port MIMO system with a lower mutual coupling. An isolating structure with a whirligig shape improves isolation, to 25 dB[11]. In antenna design, various geometric features, defects, or slots are often incorporated into the ground plane to enhance performance. Designs incorporating defective ground structures (DGS) shows the highest efficiency levels., which also offer wider bandwidth and lower mutual coupling. DGS is a key technique that improves antenna

*Corresponding author:
(E-mail: inderpreet@mjpru.ac.in)

performance can be done incorporating intentional discontinuities those are within the ground plane beneath the patch .Split-ring resonators abbreviated as SRRs and created by the process of etching of two circular or square metallic rings onto a dielectric substrate, are another approach used in antenna systems. These rings, with gaps at their opposing ends, introduce structural inhomogeneities, allowing SRRs to resonate at wavelengths those are way more longer than the ring's diameter. The gaps also generate significant capacitance, enabling resonance at frequencies higher than the physical size of the resonator would suggest, due to the relationship that is inverse in nature between capacitance & its resonant frequency .One different technique between antenna elements to minimize mutual coupling involves altering cross-admittance in the decoupling network using discrete components or transmission lines. A planar decoupling network that acts as a resonator can efficiently reduce mutual coupling. Enhancing efficiency and achieving a broadband gap-widening scattering parameter. Additionally, far-field gain patterns can be directed as needed. To further mitigate mutual coupling, neutralization methods such as transmitting electromagnetic (EM) waves through metallic slits or lumped elements between antenna elements are employed. This technique improves both antenna coupling and bandwidth. Parasitic elements, typically conductive components like metal rods, are also used to enhance antenna performance. These elements, while not electrically connected to the main antenna system, contribute to the overall design by affecting the electromagnetic field distribution[12-15].

The novelty of this work lies in the design and integration of a compact dual-band eight-port MIMO antenna system having two distinct frequency bands (9.2-9.5 GHz and 11.5-12.5 GHz) with a substrate integrated waveguide (SIW) structure and a common ground plane it versatile for various applications within these frequency ranges, such as satellite communications and radar systems. By incorporating SIW into the antenna design, the system achieves enhanced isolation (>15 dB), which is crucial for MIMO performance. This integration offers a compact solution while maintaining high isolation between ports, reducing interference and improving system reliability. The use of four identical coaxial-fed annular ring radiators, mounted on an FR4 substrate, enhances the antenna's efficiency, while the placement of the feed structure over the radiators further improves performance. This configuration ensures high gain (8 dB and 6.6 dB in the respective bands) and stable radiation patterns. The antenna exhibits an exceptionally low Envelope Correlation Coefficient (ECC) of 0.0006, indicating excellent isolation between MIMO channels. The high Diversity Gain (DG) of 9.96 dB further underscores the system's ability to maintain signal integrity and reduce fading in multipath environments, critical for robust wireless communication.

2 Design and Fabrication of the proposed antenna

The proposed antenna element consists of an annular ring with inner radius and outer radius as in Fig. 1(a). bounded inside an array of metallic via

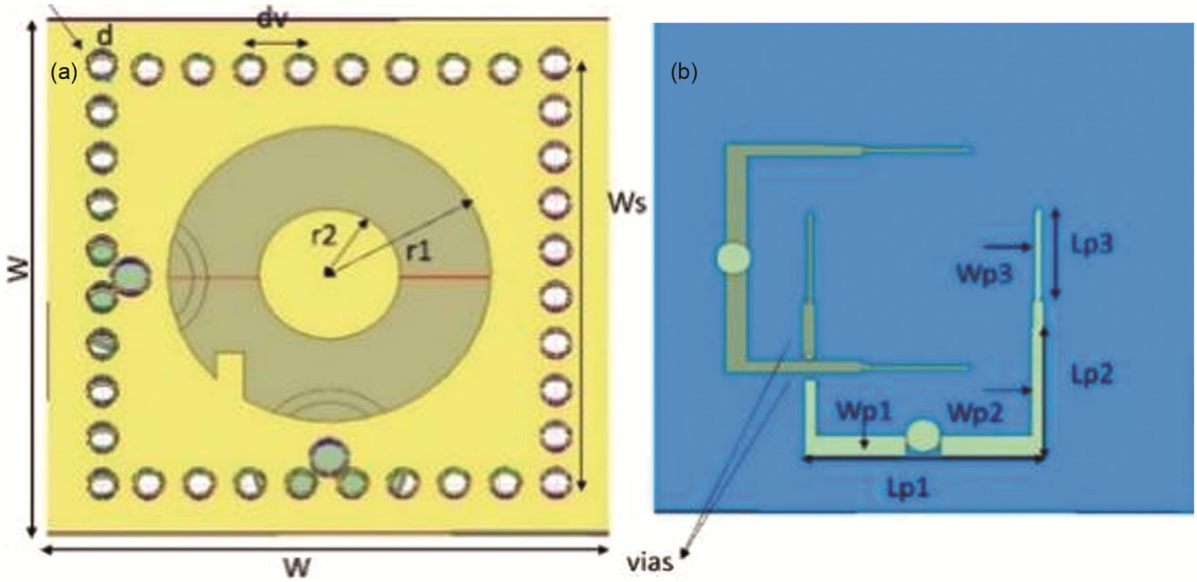

Fig. 1 — Schematic Geometry of an element (a) Top Layer (b) Bottom Layer

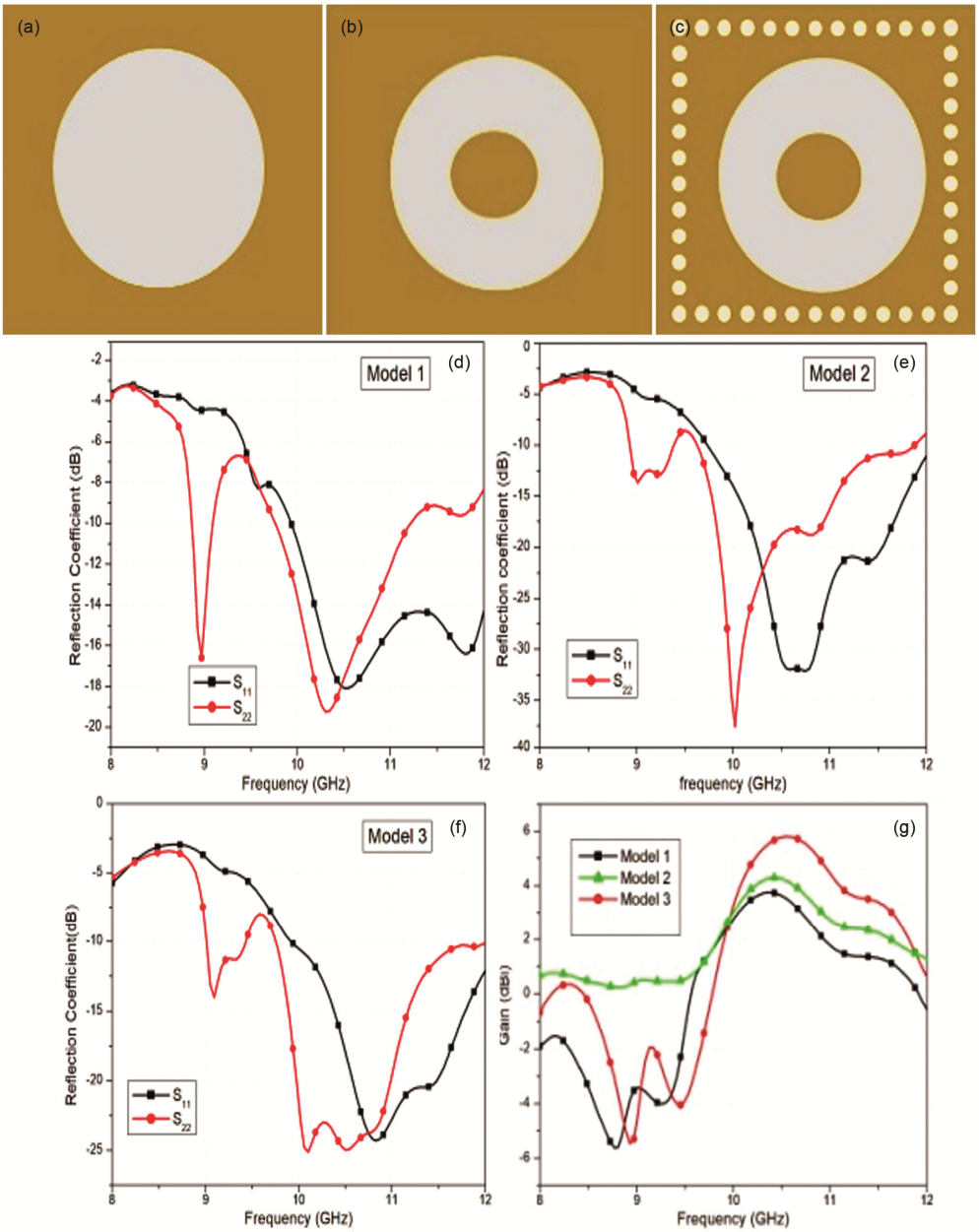

Fig. 2 — Stepwise evaluation of single radiator antenna (a) Model 1 (b) Model 2 (c) Model 3 Reflection Coefficient (d) Model 1 (e) Model 2 (f) Model 3 (g) Gain

array.The feeding structure is designed on different layer as depicted in Fig. 1(b).The antenna is fabricated on an FR4 substrate with a dielectric constant of 4.4 and surface area size of single element is 20 x 20 mm^2.

2.1 Designing sequence of the proposed antenna

We have designed the three 2 port MIMO arrays, namely Models I, II and III, and subsequently presented the models in Figs. 2(a), (b), and (c), respectively.

The model I consist of a circular slot with a radius of r1, fed by a coaxial feed on FR4 substrate with a permittivity of 4.4. However, the corresponding S11 and S22 values, shown in Fig. 2(d), indicate poor impedance matching and inadequate gain, as illustrated in Fig. 2(g).

To address these issues, we introduce Model II, a ring antenna with inner radius r2 and outer radius r1, which shows significant improvement in S11 and S22, achieving a return loss minimum of -38dB and -34dB, respectively (Fig. 2(e)). Furthermore, integrating

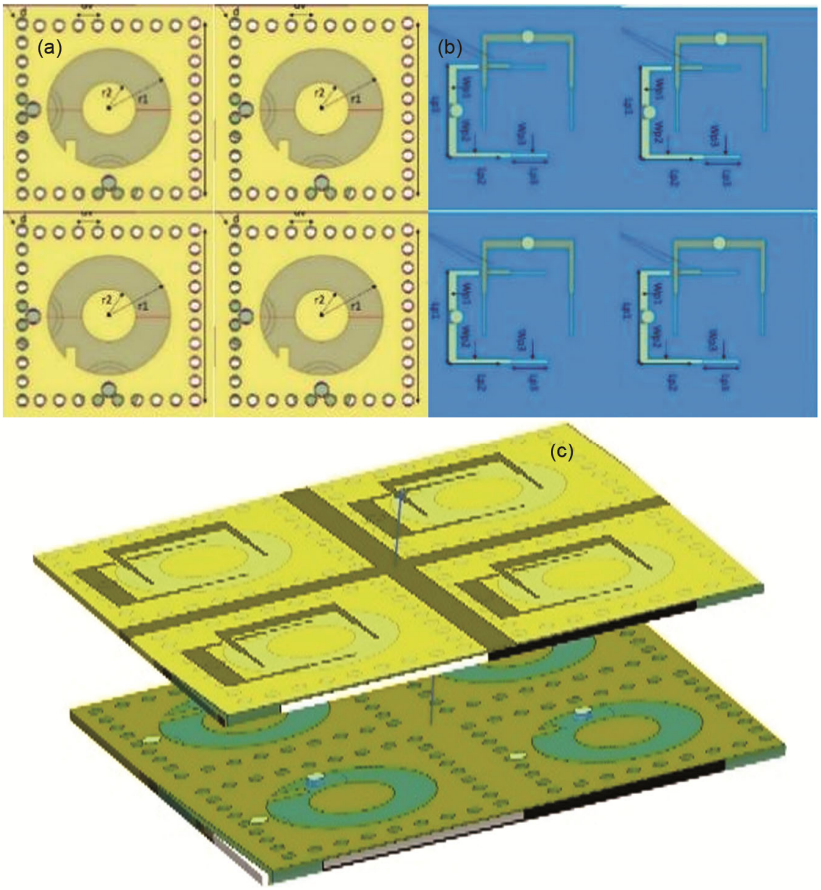

Fig. 3 — Schematic Geometry of 8-port stack antenna shown respectively as (a) Top view (b)Bottom view (c) 3D View

the ring antenna with SIW enhances bandwidth (Fig. 2(f)) and gains up to 6.5dBi (Fig. 2(g)).

2.2 Eight Port MIMO Antenna

With a circular slot, a U-shaped feedline, and a substrate-integrated waveguide (SIW) cavity, the antenna design is small, measuring only 40 mm by 40 mm as shown in Fig. 3(a & b) with the optimized dimension being listed in Table 1. This antenna features four elements and eight connectors.The SIW cavity is meticulously constructed on a FR4 substrate with a thickness of 3.2 mm and a relative permittivity of 4.4 (ε_r). Periodic metallic vias are used in this process. Interestingly, the substrate is consists of two metal layers: the bottom metal layer covers the substrate's underside, while the upper metal layer contains the circular slot. Simultaneously, the U-shaped feedline is formed onto a separate FR4 substrate layer having thickness of 0.8 mm. This substrate is placed over the circular slot with consideration. The U-shaped feedline's midpoint is directly connected to the centre conductor a standard 50Ω SMA connector positioned beneath the SIW cavity. Additionally, the outer conductor of the SMA connector establishes a link to the lower metal layer of the substrate.

Table 1 — Design Parameter abbreviated as DP Vs Calculated Value abbreviated as CV) of single-element antenna

DP	CV (λg)	DP	CV (λg)	DP	CV (λg)	DP	CV (λg)
L	0.766	W	0.766	Ws	0.6133	h	0.1226
d	0.038	dv	0.069	R2	0.115	R1	0.2298
Wp1	0.03064	Lp1	0.3351	Wp2	0.0172	Lp2	0.101
Wp3	0.01149	Lp3	0.1493				

2.3 Parametric Study

The outer radii of a ring affect the current distribution and impedance matching of the antenna. The optimized value of r1 for both ports is found at 6mm. The ratio of r1 and r2 effect the capacitance of an antenna hence the overall impedance of antenna varies with the variation in r1 & r2, hence affect the gain, a maximum gain of 6.5 dBi is found at an optimized value of r2 =3mm as depicted in Fig. 4(a & b).

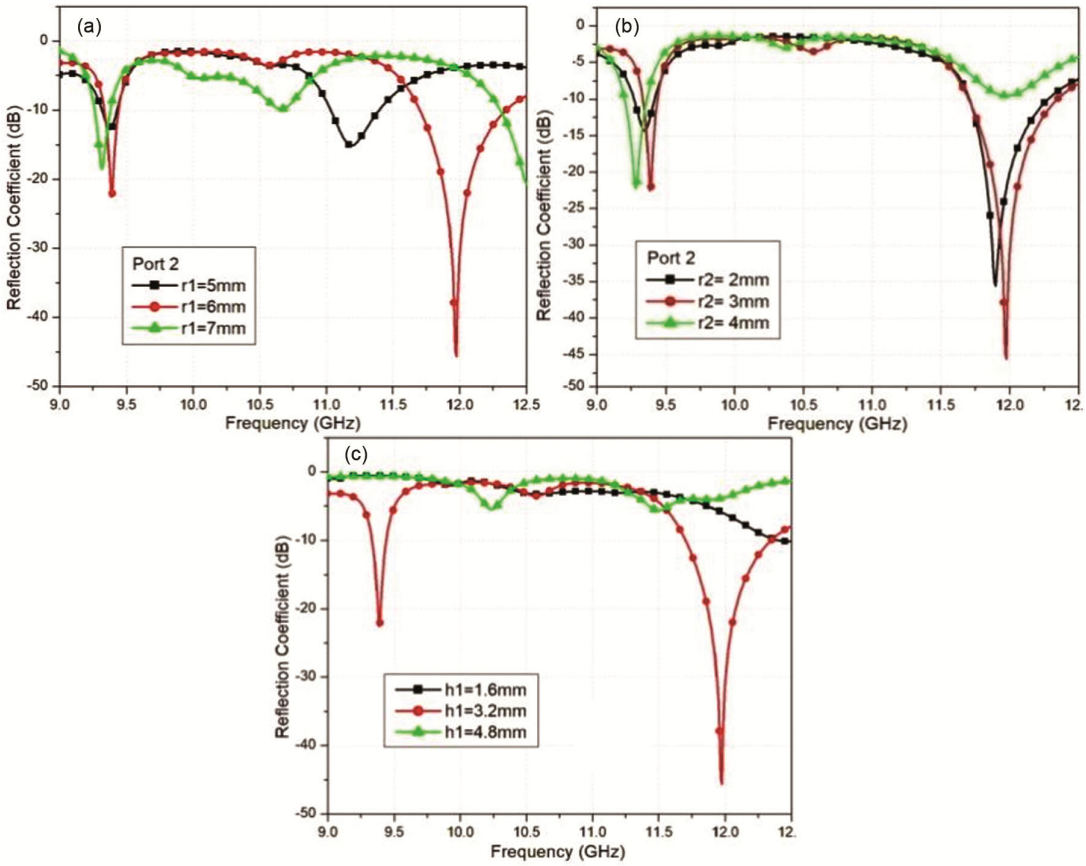

Fig. 4 — Parametric (a) variation of r1 at r2=3mm, (b) variation of r2 at r1=6mm, (c) variation of h1

Optimal 'h1' set at 3.2 mm. Based on performance, 'h2' optimized to 0.8mm. Gain improves as 'h1' decreases, but best matching at 'h1=3.2mm' presented in Fig. 4(c) The gain of a substrate-integrated waveguide (SIW) antenna can be enhanced by reducing the substrate thickness because it reduces the dielectric loss and increases the radiation efficiency. The SIW cavity also helps to improve the gain by increasing the directivity and reducing the back radiation.

2.4 Surface Current Distribution

Figure 5 displays the electric field patterns when the SIW (Substrate Integrated Waveguide) structure is employed as depicted in Fig. 5(a) clearly shows that activating all ports results in insufficient isolation between the antennas. When SIW is integrated within a structure, due to its shielding property the mutual coupling between the antenna elements get reduced as shown in surface current distribution pattern in Fig. 5(b).

2.5 Radiation Mechanism of the proposed structure.

Several metallic vias are incorporated into the design, each possessing a radius of 0.5 mm. These vias serve to establish connections between the upper surface of layer1 as well as the lower surface of layer2. Through these connections, a conducting cavity is formed, which can be analogized to the application of substrate-integrated waveguide (SIW) technology. Consequently, the presence of these vias serves a dual role. Not only do they establish connections between the parasitic ground and the lower ground plate, thereby enhancing the antenna's gain, but they also significantly enhance the isolation between two distinct elements.

The radiated wave originating from the slot progresses toward two edges, thereby engendering an in-phase electric field within the via. The gain of this fundamental element is augmented due to the constructive superposition of electric fields that are in phase. An in-phase electric field refers to a scenario where the oscillations of the electric field vectors of different waves align perfectly or coincide with each other. When these electric fields are in phase, they amplify each other's strength through constructive interference. In the context of the described mechanism, as the radiated wave travels along the

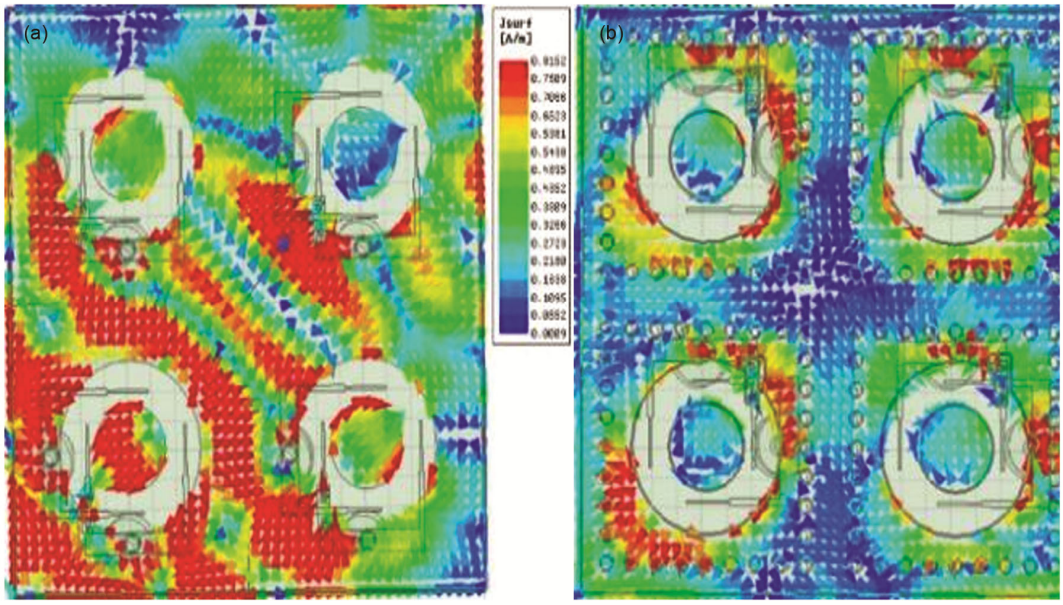

Fig. 5 — Surface Current distribution (a) Without SIW (b) With SIW

SIW slot and interacts with the edges, the resulting electric fields are generated within the via alignment in such a way that their combined effect reinforces the overall electric field strength. This alignment results in a more concentrated and intensified electric field distribution, leading to gain enhancement in the antenna's basic element. To attain the desired in-phase effect within the via, it is imperative to meticulously engineer the dimensions of wg (waveguide width) and dv (distance between via). As evidenced by Fig. 6, the introduction of an SIW cavity does not notably alter the reflection coefficient of the antenna; however, a marginal downward shift is observed in isolation. Notably, the peak gain experiences a significant enhancement, increasing from 4dBi-6 dBi upon the integration of the SIW structure shown in Fig. 6.

3 Results and Discussion

3.1 Scattering Performance

Fig. 6(a & c) present the reflection coefficient of the proposed work with and without SIW respectively in which integration of SIW enhances the impedance matching. Fig. 6(b & d) presents the Isolation of the proposed structure with and without SIW.The gain of the proposed structure enhances to 8.8 dBi at lower band and 7dBi at higher band when SIW is integrated as depicted in Fig. 6(e)

3.2 Radiation performance

Antenna is placed in an anechoic chamber (to avoid reflections) or an open field test range. Place the AUT on a rotatable platform to allow for measurement at different angles. Connect the AUT and reference antenna to a network analyzer or a similar measurement device. Perform a calibration to ensure the accuracy of the measurements. This involves measuring the response of the reference antenna and adjusting the system accordingly. Rotate the AUT in small increments (e.g., 1° or 5°) and measure the received signal strength at each angle. Capture the magnitude and phase of the received signal at each angle. This can be done in both the azimuth (horizontal) and elevation (vertical) planes. Normalize the measured data to account for any variations in the measurement setup. Use the normalized data to plot the radiation pattern in polar or Cartesian coordinates. This will show the directional characteristics of the antenna. For co-polarization Record the received signal strength at the reference antenna when it is aligned with the AUT's intended polarization. Rotate the reference antenna by 90 degrees to measure the cross-polarization. For a vertically polarized AUT, the reference antenna should be horizontally polarized. The figure illustrates the simulated as well as measured radiation patterns for port 1 in a MIMO antenna structure. The antenna's far-field characteristics were measured in an anechoic chamber, with radiation patterns shown for both co-polarization and cross-polarization at frequencies of 9.2 GHz and 11.8 GHz. A standard gain horn antenna was used as the transmitting antenna (Tx), while the antenna under test served as the receiving antenna (Rx). Amplifiers

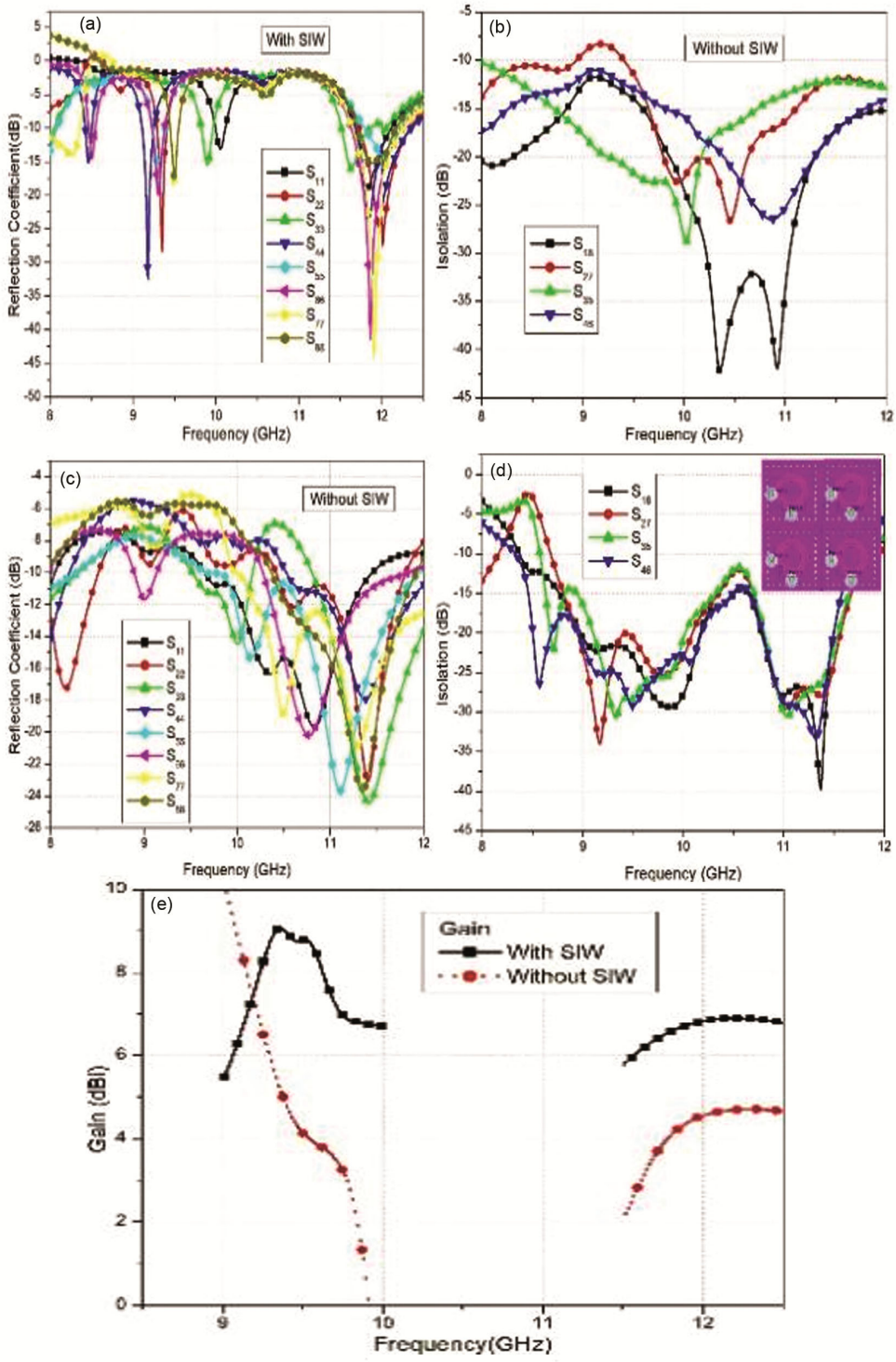

Fig. 6 — Without SIW (a) Reflection Coefficient (b) Isolation, With SIW (c) Reflection Coefficient (d) Isolation (e) gain

were used to maintain steady power reception during the measurements. The tested antenna was rotated systematically to gather data at various orientations. The 3 dB angular beam-width at 9.2GHz is 27°, while at 11.8 GHz it is 31°

The antenna demonstrates a broadside radiation pattern oriented in the +z direction. Fig. 7(a & b) illustrates the simulated radiation patterns in the xz-plane at 9.2 GHz and 11.8 GHz and Fig. 7(c & d) presents in the yz-plane when all ports are excited.

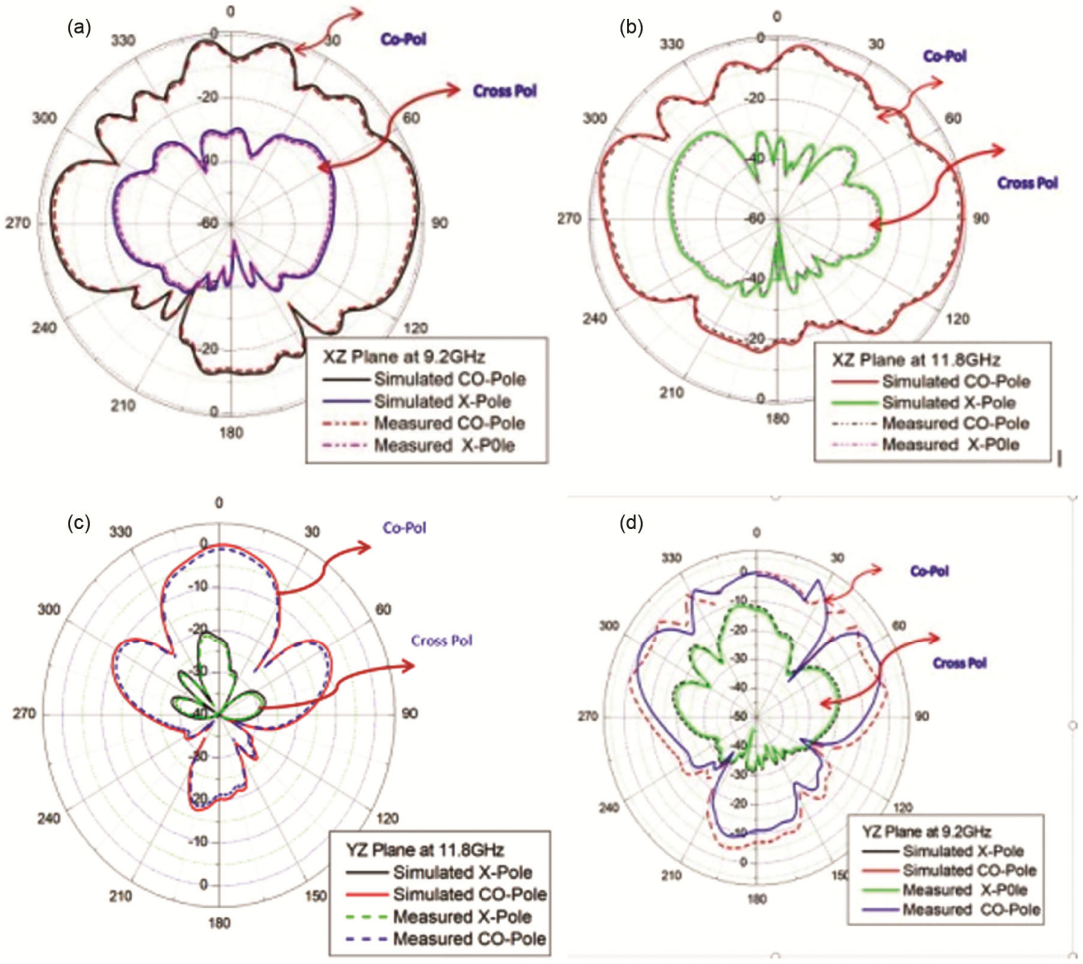

Fig. 7 — At Frequency 9.2 GHz (a) XZ Plane (b) YZ Plane, At Frequency 11.8 GHz (c) XZ Plane (d) YZ Plane

Integration of SIW maintains positive gain across the operating bandwidth. SIW cavity-backed slot antennas can use the SIW cavity to reduce the surface current and back lobe radiation and to excite higher resonance modes, which can improve the antenna gain.

3.3 Diversity Performance

The efficacy of the suggested antenna inside a MIMO (Multiple Input, Multiple Output) system is based on certain fundamental diversity characteristics. Including the envelope correlation coefficient (ECC), diversity gain (DG), and channel capacity loss (CCL). The ECC specifically denotes the degree to which the radiation pattern of one antenna matches that of another when they are utilized in close proximity. A high ECC value inhibits the antenna's MIMO performance. For MIMO antennas to work well, it is generally advisable to have an ECC value below 0.5. ECC is calculated using the S parameter as

$$\text{ECC} = \rho(i,j,N) = \frac{\left|\left(\sum_{n=1}^{N}\{S_{in}^{*}S_{nj}\}\right)\right|^{2}}{\prod_{k=i,j}\left(1-\sum_{n=1}^{N}\{S_{kn}^{*}S_{nk}\}\right)} \quad \ldots(1(a))$$

The far-field radiation pattern technique utilizes azimuthal and elevation radiated field components for the i-th and j-th elements, respectively. These parameters are obtained using an anechoic chamber, and the results are expressed as correlation coefficients using this method.

$$Pij(e) = \frac{\left|\iint_{4\pi} F_i(\theta,\phi)XF_j(\theta,\phi)d_\Omega\right|}{\iint_{4\pi}|F_i(\theta,\phi)|d_\Omega \iint_{4\pi}|F_j(\theta,\phi)|d_\Omega} \quad \ldots.(1b)$$

Where (θ,) and (θ,) are field patterns of two radiating elements with respect to θ, the evaluation using implies the computation of the radiation pattern at each frequency. This method is regarded as the most precise and reliable for ECC calculation

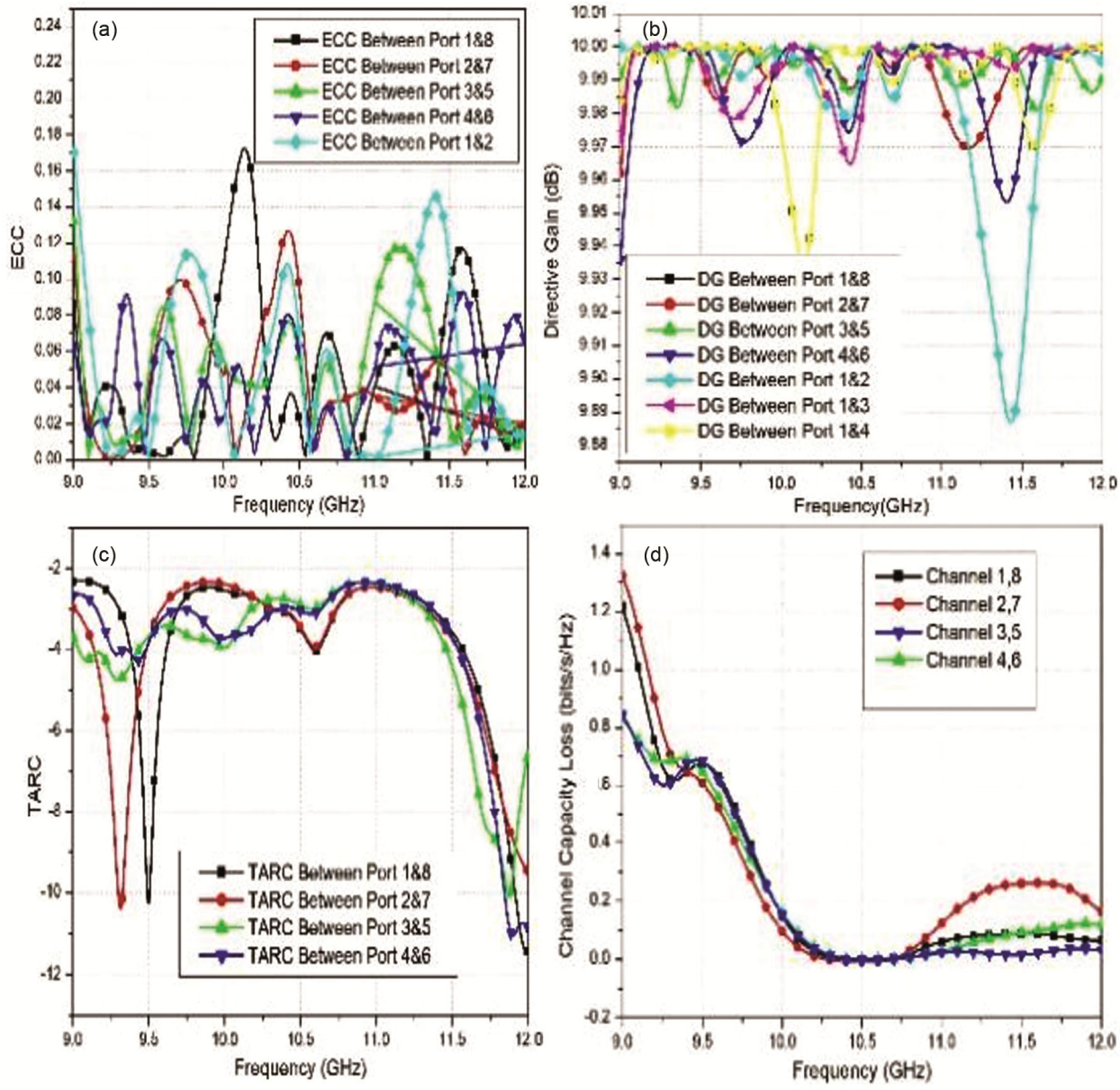

Fig. 8 — (a)ECC (b) DG, (c) TARC, (d) CCl

with any number of antenna elements. However, its primary limitation is the need for a 3D far-field radiation pattern for each antenna element, which can be time-consuming. Furthermore, it requires a complex and costly measurement setup. Where i, j are any two ports and N=8

The MIMO antenna's diversity performance is demonstrated by DG, which may be assessed using ECC.

$$DG = 10\sqrt{(1 - |ECC|^2)} \quad ...(2)$$

Figures 8(a & b) depict simulated ECC and DG charts. It can be seen that for 11.5–12GHz, the DG is greater than 9.8 dB and the ECC results are significantly below 0.18. Channel Capacity Loss, or CCL, limits the maximum data transfer rate that can be sent via a channel. A larger possible data transfer rate is implied by a lower CCL value. To guarantee optimal performance in a MIMO (Multiple Input, Multiple Output) system, the CCL should normally be less than 0.4 bits per second per Hertz (bits/s/Hz). For the proposed antenna it is less than 0.3 as shown in Fig. 8(d).

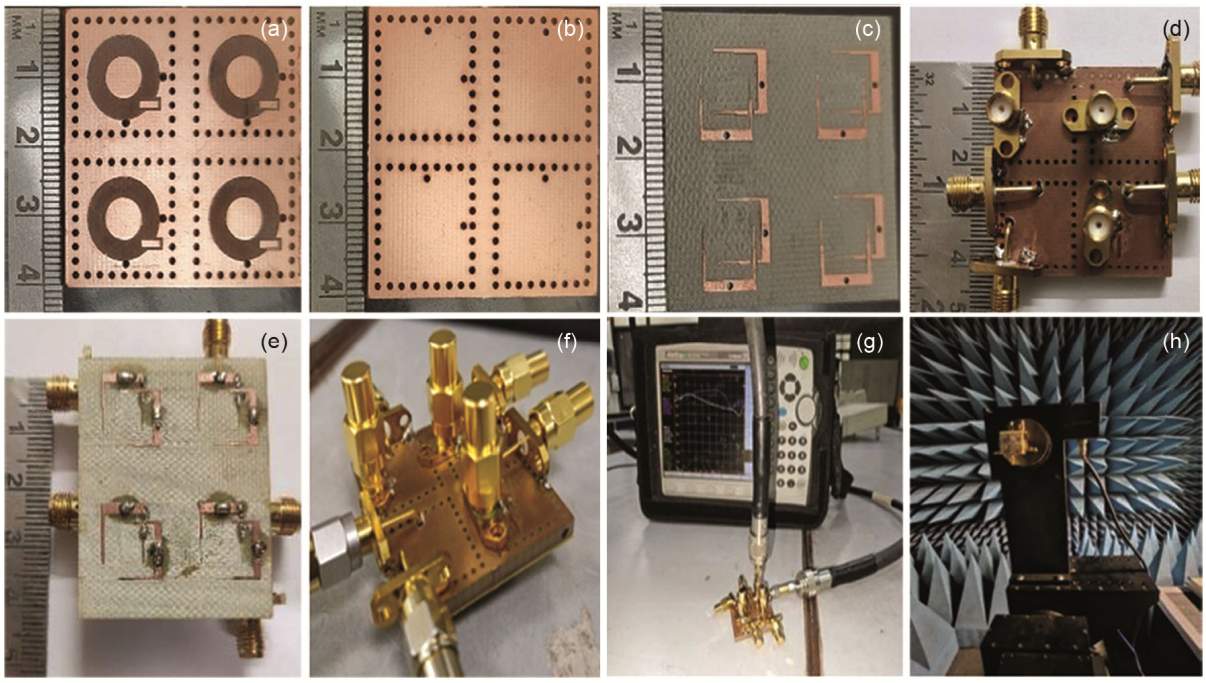

Fig. 9 — First layer (a) front view (b) bottom view, second layer (c) front view, Prototype (d) bottom view (e) front view (f)50Ω impedance (g)VNA measurement set up (h) Anechoic chamber set up

Analysing CCL entails determining how it affects the channel's capacity for data transfer. The Channel Capacity (CC) of the proposed 8-element MIMO is calculated using Eq. 3.

$$CC = E\left[log_2\left[\det\left(I + \eta\frac{SNR}{K}HH^H\right)\right]\right]$$

$$CCL = log_2 \det \psi_R \quad (3)$$

$$\psi_R = \begin{pmatrix} \psi_{11} & \cdots & \psi_{18} \\ \vdots & \ddots & \vdots \\ \psi_{81} & \cdots & \psi_{88} \end{pmatrix} \quad ...(4)$$

$$\psi_{ii} = \left(1 - \sum_{i,j=1}^{8} |S_{ij}|^2\right) \quad ...(5)$$

$$\psi_{ij} = -\left(S_{ii}^{*\backslash} S_{ij} + S_{ji}^{*} S_{ij}\right) \quad ...(6)$$

The square root of the total reflected power divided by the square root of the total incident power is the Total Active Reflection Coefficient (TARC) as depicted in Fig. 8(c), which measures the combination of random signals and port coupling. Over the operational band, the TARC in the suggested arrangement stays below -5dB.

3.4 Prototype and Experimental Set-up

Figure 9(a-e) displays the prototype fabrication of the proposed structure , that the two-layer antenna is designed, first layer of FR4 having a thickness of 3.2mm and the second layer is FR4 of thickness 0.5mm, the two layers are one over another without any gap. Fig. 9(f) presents when instead of excited port all other ports are terminated by 50ohm impedance. The connectors are arranged such that the gap distance between connectors must be 20mm so that VNA probes can be connected properly as shown in Fig. 9(g) . Fig. 9(h) presents the anechoic chamber set up of the proposed antenna.The difference of 0.5 dB between the simulated and measured gain is attributed to fabrication loss and cabling error.The experimental values >-10dB from 9-9.35 GHz and 11.5-12.25 GHz, resonating at 9.2 GHz and 11.8 GHz encompassing dual band with a min magnitude of -32dB, indicate good agreement between the simulated and experimental S11is, as shown in Fig. 10(a). The comparison of simulated and experimental measurements of S12 and S15 parameters is shown in Figures 10(b & c), respectively. The isolation is below -25dB.The simulation and experimental result demonstrates satisfactory level of similarity for the S parameters. The performance of the proposed antenna is compared with that of the previously published works and presented in Table 2.

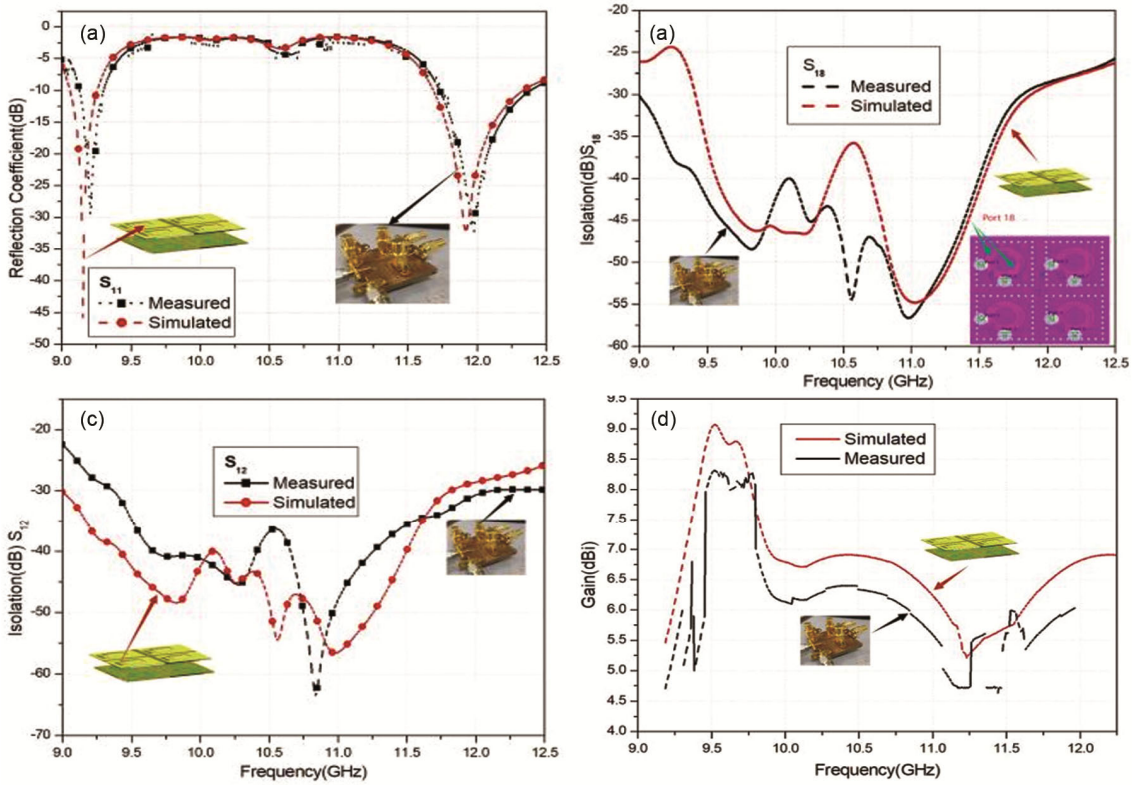

Fig. 10 — (a) Reflection Coefficient, Isolation (b) S12, (c) S15, (d) Gain

Table 2 — Comparison of proposed work with previously published work

Ref. No	Size mm^3	MC Tech	BW (GHz)	Gain dBi	ports	Mutual Coup-ling (dB)	ECC
[16]	2x60.4x0.8	MCM	3.4-3.6	--	8	<16.7	<0.1
[17]	76x19x4	One branch mono pole	3.4-3.6 4.8-5.0	--	8	<12	--
[18]	0.112	SIW	6.006-6.143	4.72	8	<21.17	<0.0027
[19]	120x50 x2.2	Probe &Resonato	2.25-2.63 5.14-6.06	4	2	<-15	-
[20]	33x33x1.6	FSS	7.8-9.08	5.2	4	<-20	0.005
Proposed	40x40x4	SIW	9-9.5 11.5-12.25	6.6 8	8	<-15	<0.10 <0.14

4 Conclusion

This paper presents a novel MIMO antenna design that incorporates a Substrate Integrated Waveguide (SIW) annular ring radiator and a layered feeding structure to enhance overall performance. The antenna operates at dual frequencies of 9.2 GHz and 11.8 GHz, demonstrating key features such as high gain (8 dB and 6.6 dB), a low Envelope Correlation Coefficient (ECC) of 0.10, and a high Diversity Gain (DG) of 9.97. The enhanced radiation characteristics and diversity performance are mostly attributed to these qualities.To achieve optimal isolation and gain, a distinct feeding structure is deployed on separate layers, resulting in consistent resonance frequencies at 9.2 GHz and 11.8 GHz. The measured and simulated results show close agreement, validating the design. This approach offers a promising solution for improving MIMO antenna performance, making it suitable for millimeter-wave applications and addressing current limitations in MIMO systems.

References

1 Li C, Zhu H, Cai J, Hu J & Li G, *IEEE Trans Veh Technol*, 70 (2021) 4435.
2 Eslami A, Nourinia J, Ghobadi C & Shokri M, *Int J Microwave Wireless Technol*, 13 (2021) 859.
3 Li M, Zhang Y, Wu D, Yeung K L, Jiang L & Murch R, *IEEE Trans Antennas Propag*, 70 (2022) 1764.
4 Li M & Cheung S, *IEEE Trans Veh Technol*, 70 (2021) 446.

5 Yang W, Chen L, Pan S, Che W & Xue Q, *IEEE Trans Antennas Propag*, 70 (2022) 2686.

6 Li M, Zhong B & Cheung S W, *IEEE Trans Antennas Propag*, 67 (2019) 755.

7 Diman A, Karami F, Rezaei P, Amn-e-Elahi A, Razi Z M, Denidni T A & Kishk A A, *IEEE Trans Antennas Propag*, 69 (2021) 6058.

8 Karami F, Rezaei P, Amn-e-Elahi A & Abolfathi A & Kishk A A, *Int J RF Microw Comput.-Aided Eng*, 31 (2021) e22772.

9 Amn-E-Elahi, Rezaei P, Karami F, Hyjazie F & Boutayeb H, *IEEE Trans Antennas Propag*, 70 (2022) 12253.

10 Rekha S, Ramson J & Parasitically S R, *Arab J Sci Eng*, 47, (2022) 14711.

11 Kulkarni J, Sim C Y D, Desai A, *et al.*, Arab J Sci Eng, 47 (2022) 14087.

12 Sharawi M S, Ikram M & Shamim A, *IEEE Trans Antennas Propag*, 65 (2017) 6679.

13 Li Z, Du Z & Gong K, A Dual-Slot Diversity Antenna withIsolation Enhancement Using Parasitic Elements for mobile Handsets, *Asia Pacifc Microwave Conference*, Singapore, 2021.

14 Zhao X, Yeo S P & Ong L C, *IEEE Trans Antennas Propag*, 66 (2018) 420.

15 Tiwari P, Rai J K, Gahlaut V & Ranjan P, *AEU - Int J Electron Commun*, 178 (2024) 155280.

16 Fang Y, Jia Y, Zhu J-Q, Liu Y & An J, *IEEE Trans Antennas Propag*, 72 (2024) 1905.

17 Deng C, Cao X, Li D & Yu W, *IEEE Antennas Wireless Propag Lett*, 22 (2023) 1281.

18 Mishra M, Chaudhuri S, Kshetrimayum R S, Sharawi M S & Kishk A A, *IEEE Antennas Wireless Propag Lett*, 22 (2023) 1721.

19 Zhang W, Li Y, Wei K & Zhang Z, *IEEE Trans Antennas Propag*, 71 (2023) 5749.

20 Khan I, Zhang K, Ali L & Wu Q, *IEEE Antennas Wireless Propag Lett*, 22 (2023) 2836.